Tuberculosis 126 (2021) 102043

Contents lists available at ScienceDirect

Tuberculosis

journal homepage: http://www.elsevier.com/locate/tube

Metabolic profiles of multidrug resistant and extensively drug resistant *Mycobacterium tuberculosis* unveiled by metabolomics

Amanda Mendes Rêgo [a,b], Duanne Alves da Silva [a], Nicole Victor Ferreira [a], Lucindo Cardoso de Pina [a], Joseph A.M. Evaristo [c], Geisa P. Caprini Evaristo [c], Fabio Cesar S. Nogueira [c], Soraya M. Ochs [d], Julio J. Amaral [d], Rosana B.R. Ferreira [e], L. Caetano M. Antunes [a,f,*]

[a] *Escola Nacional de Saúde Pública Sergio Arouca, Fundação Oswaldo Cruz, Brazil*
[b] *Instituto Oswaldo Cruz, Fundação Oswaldo Cruz, Brazil*
[c] *Instituto de Química – LADETEC, Universidade Federal do Rio de Janeiro, Brazil*
[d] *Instituto Nacional de Metrologia, Qualidade e Tecnologia, Brazil*
[e] *Instituto de Microbiologia Paulo de Góes, Universidade Federal do Rio de Janeiro, Brazil*
[f] *Instituto Nacional de Ciência e Tecnologia em Doenças de Populações Negligenciadas, Centro de Desenvolvimento Tecnológico em Saúde, Fundação Oswaldo Cruz, Brazil*

ARTICLE INFO

Keywords:
Drug resistance
Mycobacterium tuberculosis
Metabolic profile
Metabolomics

ABSTRACT

Although treatable with antibiotics, tuberculosis is a leading cause of death. *Mycobacterium tuberculosis* antibiotic resistance is becoming increasingly common and disease control is challenging. Conventional drug susceptibility testing takes weeks to produce results, and treatment is often initiated empirically. Therefore, new methods to determine drug susceptibility profiles are urgent. Here, we used mass-spectrometry-based metabolomics to characterize the metabolic landscape of drug-susceptible (DS), multidrug-resistant (MDR) and extensively drug-resistant (XDR) *M. tuberculosis*. Direct infusion mass spectrometry data showed that DS, MDR, and XDR strains have distinct metabolic profiles, which can be used to predict drug susceptibility and resistance. This was later confirmed by Ultra-High-Performance Liquid Chromatography and High-Resolution Mass Spectrometry, where we found that levels of ions presumptively identified as isoleucine, proline, hercynine, betaine, and pantothenic acid varied significantly between strains with different drug susceptibility profiles. We then confirmed the identification of proline and isoleucine and determined their absolute concentrations in bacterial extracts, and found significantly higher levels of these amino acids in DS strains, as compared to drug-resistant strains (combined MDR and XDR strains). Our results advance the current understanding of the effect of drug resistance on bacterial metabolism and open avenues for the detection of drug resistance biomarkers.

1. Introduction

Tuberculosis (TB) is a major public health issue and a leading cause of death worldwide. Drug resistance adds to this problem, and multidrug-resistant (MDR) TB cases are increasingly common [1,2]. Phenotypic drug susceptibility testing (DST) of *M. tuberculosis* is long and laborious, causing late diagnosis and failed therapy [3]. Two culture-based DST methods are routinely used: the proportions method, which takes ≥21 days and the BD BACTEC MGIT Automated Mycobacterial Detection System, which takes 6–13 days [4,5]. Due to such long wait periods, treatment often needs to be initiated empirically, contributing to treatment failure. The treatment of drug-susceptible (DS) infections takes at least six months, also promoting high treatment default rates and the emergence of drug-resistant (DR) strains [6]. Exposure of *M. tuberculosis* to sub-optimal antibiotic concentrations during treatment favors the selection of mutations that provide drug resistance but also impact physiology, and DR bacteria may suffer 'fitness costs', such as reductions in virulence, transmission, and growth [7], although compensatory mutations may be selected [8–10]. Therefore, metabolic changes elicited by drug resistance mutations may be used to predict drug resistance without the need for DST [11–13]. To this end, one tool that could aid in drug resistance prediction is

* Corresponding author. National School of Public Health, Oswaldo Cruz Foundation, Rio de Janeiro - RJ, Brazil.
E-mail address: caetano.antunes@fiocruz.br (L.C.M. Antunes).

https://doi.org/10.1016/j.tube.2020.102043
Received 27 September 2020; Received in revised form 23 November 2020; Accepted 15 December 2020
Available online 24 December 2020

metabolomics, the analysis of the chemical complexity within biological samples [14]. Over the last several years, we used high-throughput metabolomics to probe the chemical composition of various sample types, and found that the metabolic fingerprints produced can help distinguish states of health and disease [15–24]. Therefore, we hypothesized that mutations leading to *M. tuberculosis* drug resistance cause metabolic alterations that could be detected by metabolomics. Here, we describe the use of metabolomics to characterize a set of DS, MDR, and extensively drug-resistant (XDR) *M. tuberculosis* strains. Our data show that drug susceptibility can be partially predicted using relative abundances of the metabolites found, sheding light on the metabolic effects of drug resistance in *M. tuberculosis*. Additionally, our findings may pave the way for the identification and validation of biomarkers for the rapid diagnosis of DR TB.

2. Materials and methods

2.1. M. tuberculosis strains

Fifty-three strains from the strain collection of the National Reference Laboratory in Tuberculosis and Other Mycobacterioses Ângela Maria Werneck (Oswaldo Cruz Foundation, Brazil) were used. *M. tuberculosis* complex identification was performed using the SD BIOLINE TB Ag MPT64 Rapid test (Standard Diagnostics, Yongin, Korea).

2.2. Drug susceptibility testing

Strains were grown in Löwenstein Jensen (LJ) medium (Becton, Dickinson & Company, Franklin Lakes, USA). After incubation for ~20 days at 37 °C, DST was performed using the BD BACTEC MGIT Automated Mycobacterial Detection System (Becton, Dickinson & Company) following standard procedures. First-line drug concentrations were 1 μg/mL for streptomycin and rifampicin, 0.1 μg/mL for isoniazid, and 5 μg/mL for ethambutol (Becton, Dickinson & Company). Second-line drugs were used at 1 μg/mL for amikacin, 2 μg/mL for ofloxacin, 5 μg/mL for kanamycin and 2.5 μg/mL for capreomycin (Sigma-Aldrich, St. Louis, USA).

2.3. Mutation analysis

Target genes were PCR-amplified and sequenced in a 3130 Genetic Analyzer (Applied Biosystems, Foster City, USA). Primer sequences and amplification conditions are shown in Table S1. Sequencing results were compared with *Mycobacterium tuberculosis* H37Rv sequences using online (NCBI, https://www.ncbi.nlm.nih.gov/) and offline tools (ApE A Plasmid Editor, http://jorgensen.biology.utah.edu/wayned/ape/).

2.4. Metabolite extraction

Strains were grown on LJ for 28 days at 37 °C. Colonies were transferred to vials with 2 mL of 7H9 broth supplemented with oleic acid, albumin, dextrose and catalase and glass beads, and vortexed. Bacterial suspensions were diluted 1:200 in 7H9 broth and the optical density (600 nm) was measured. Different culture volumes were centrifuged (4 min at 11,500 g), the supernatant discarded, and the pellet resuspended in 500 μL of acetonitrile (≥99.9%, Sigma-Aldrich). Volumes were calculated so that final ODs would be 5. Resuspended pellets were vortexed and kept in an ultrasonic bath for 3 min. Samples were centrifuged for 4 min at 11,500 g and the supernatant was collected, filtered (0.22-μm), and stored (−20 °C).

2.5. Direct infusion mass spectrometry (DI-MS)

Extracts produced as described above were dried using a speedvac, resuspended in 1 mL of 60% acetonitrile (≥99.9%, Sigma-Aldrich), kept in an ultrasonic bath for 5 min, and centrifuged (14,000 g, 30 min) at 6 °C. For positive ionization mode 0.1% formic acid was added; 0.5% ammonium hydroxide was added for negative mode. Quality control was performed by injecting a mixture of samples at the beginning and end of analyses, as well as after groups of 10 samples. Mass calibration (50–2000 *m/z*) was performed with a phosphoric acid solution. Samples were directly infused (randomly) into a Synapt G1 High Definition Mass Spectrometer (Waters, Milford, USA) at 10 μL/min. Scan range was 100–1000 *m/z* for 5 min in dynamic mode and scan time of 0.8 s. Positive mode was performed with capillary, sampling and extraction voltages at 3.2 kV, 30 V and 5 V. Source parameters for negative mode were 3 kV in the capillary, and cone of sampling and extraction at 50 and 6 V. Other parameters included source temperature at 80 °C, desolvation temperature at 100 °C, 380 L/h gas flow and collision cell voltage at 6 V.

2.6. DI-MS data processing

MS data were acquired using MassLynx v.4.1 (Waters) and processed with MassLynx and MarkerLynx XS. Raw data were transformed to centroid mode using the "Accurate Mass Measure" tool, and resulting mass data were processed with MarkerLynx, using the parameters: "analysis type" = "combined scan range", "peak separation" (Da) = 0.02 and "marker intensity threshold (counts)" = 3,000, 6000 or 12,000. A two-dimensional data table (*m/z* versus peak intensity) was generated for each sample group.

2.7. Ultra-High-Performance Liquid Chromatography and High-Resolution Mass Spectrometry (UHPLC-HRMS)

Initially, 100 μL of each sample in acetonitrile (≥99.9%, Fluka Analytical, Charlotte, USA) were dried and reconstituted in 200 μL of 5% methanol (99%, Tedia High Purity Solvents, Fairfield, USA). Quality control was performed with a mixture of samples (10 μL each) in 200 μL of 5% methanol, injected after each group of 7 samples. Mass measurements were calibrated using a calibrant solution (Thermo Scientific, Waltham, USA) containing caffeine, MRFA, and Ultramark 1621, from 195 to 1522 *m/z* before acquisitions. In addition, a control sample of evaporated acetonitrile reconstituted in 200 μL of 5% methanol was injected. Samples were analyzed in triplicate by UHPLC-HRMS. Briefly, metabolites were purified and concentrated using an online C_{18} enrichment column (Zorbax; rapid resolution HT 2.1 × 50 mm, pore size 1.8 μm; Agilent, Santa Clara, USA). Chromatographic separation was performed on reverse phase using a 15-min gradient with solvents B (methanol, 0.1% formic acid) and A (ultrapure water, 0.1% formic acid, 5 mM ammonium formate): 0–1 min, 5% B; 9 min, 60% B; 10 min, 100% B; 12 min, 100% B; 13 min, 5% B; 15 min, 5% B, at 500 μL/min. Metabolites were eluted directly into the high-resolution mass spectrometer (Q Exactive Plus Hybrid Quadrupole-Orbitrap MS, Thermo Scientific). Data were acquired in positive electrospray mode, with cone voltage at +3.9 kV. Sheath gas was 10 L/h, capillary temperature was 320 °C, and S-lens RF level was 50. Desolvation gas was high-purity N_2 at 5 L/h at 50 °C. Scan range was 67 to 1000 *m/z*, as profile mode, with resolution of 70,000 on FullMS. Automatic gain control (AGC) was 10^6, and maximum injection time (IT) was 50 ms. MS^2 were acquired as data-dependent analysis (DDA), using the 15 most abundant *m/z*, with 17,500 resolution, centroid, AGC 10^5 and maximum IT 100 ms. Isolation window of 2.0 *m/z* and offset of 0.5 *m/z* were used. Collision energy (CE) was stepped to 10/15/30 eV.

2.8. UHPLC-HRMS data processing and metabolite identification

UHPLC-HRMS spectra were acquired using Xcalibur 3.2 (Thermo Scientific). Data processing, analysis and metabolite identification were performed with Compound Discoverer 2.1 (Thermo Scientific) using the Categorical Factor to identify different sample groups and calculate ratios. The software workflow chosen was "Untargeted Metabolomics with

Statistics Detect Unknowns with ID using Online Databases". For putative identifications, databases were ChEMBL, *E. coli* Metabolome Database, Human Metabolome Database, KEGG, LipidMAPS, MassBank and Metabolights.

2.9. Quantification of amino acids by selected reaction monitoring (SRM)

Initially, 300 μL of samples in acetonitrile (>99.9% pure, Fluka Analytical) were dried and reconstituted in 600 μL of 5% methanol (99% pure, Tedia High Purity Solvent). Samples were analyzed in triplicate by ultra-high-performance liquid chromatography coupled with mass spectrometry (UHPLC-MS). Metabolites were purified and concentrated using the chromatographic settings described above. Metabolites were eluted directly into the mass spectrometer (TSQ Quantiva Triple-Stage Quadrupole, Thermo Scientific). Data were acquired in positive electrospray ion mode with 3.5 kV. Sheath gas was 40 L/h, auxiliar gas was 10 L/h, sweep gas was 2 L/h, capillary temperature was 350 °C and vaporizer temperature was 400 °C. Detection and quantification of proline (*m/z* 70.17) and isoleucine (*m/z* 86.18) were performed based on ion fragmentation in MS^2 mode using SRM of the 3 most intense transitions for each compound. Metabolites were quantified using calibration curves corresponding to their precursors and GABA (*m/z* 87.11) was used as internal standard. Samples were also spiked with GABA (0.01 ng/mL) as internal standard and amino acids were quantified based on signal intensities in a dweel time of 500 ms, with trigger acquisition upon detection of their transitions trace in a window of 8 min. Additionally, RF lens was set to 66, quadrupole 1 and 3 resolution were 0.7 (FWHM), and CID gas in collision chamber was 1.5 mTor. Concentrations of proline and isoleucine in samples were calculated based on their most intense transition.

2.10. Statistical data analyses

Hierarchical clustering was carried out in MetaboAnalyst (htpp://www.metaboanalyst.ca/) based on degree of similarity of abundance profiles of metabolites with the highest discriminatory power between groups, to produce dendrograms. Clustering was generated using Euclidean distances and the Ward algorithm.

Additionally, the dataset was manually analyzed using Microsoft Excel and GraphPad Prism 7 to compare the relative abundance of select ions between sample groups. Mean intensities were calculated for each group and ratios between means were obtained. Student's t-tests were performed, and $p < 0.05$ was used for statistical significance.

3. Results and discussion

Metabolomics studies have furthered our knowledge of the biology of various organisms, how they respond to perturbations, how mutations alter metabolic functions, and how these changes correlate with health or disease. For instance, we have previously used DI-MS to characterize

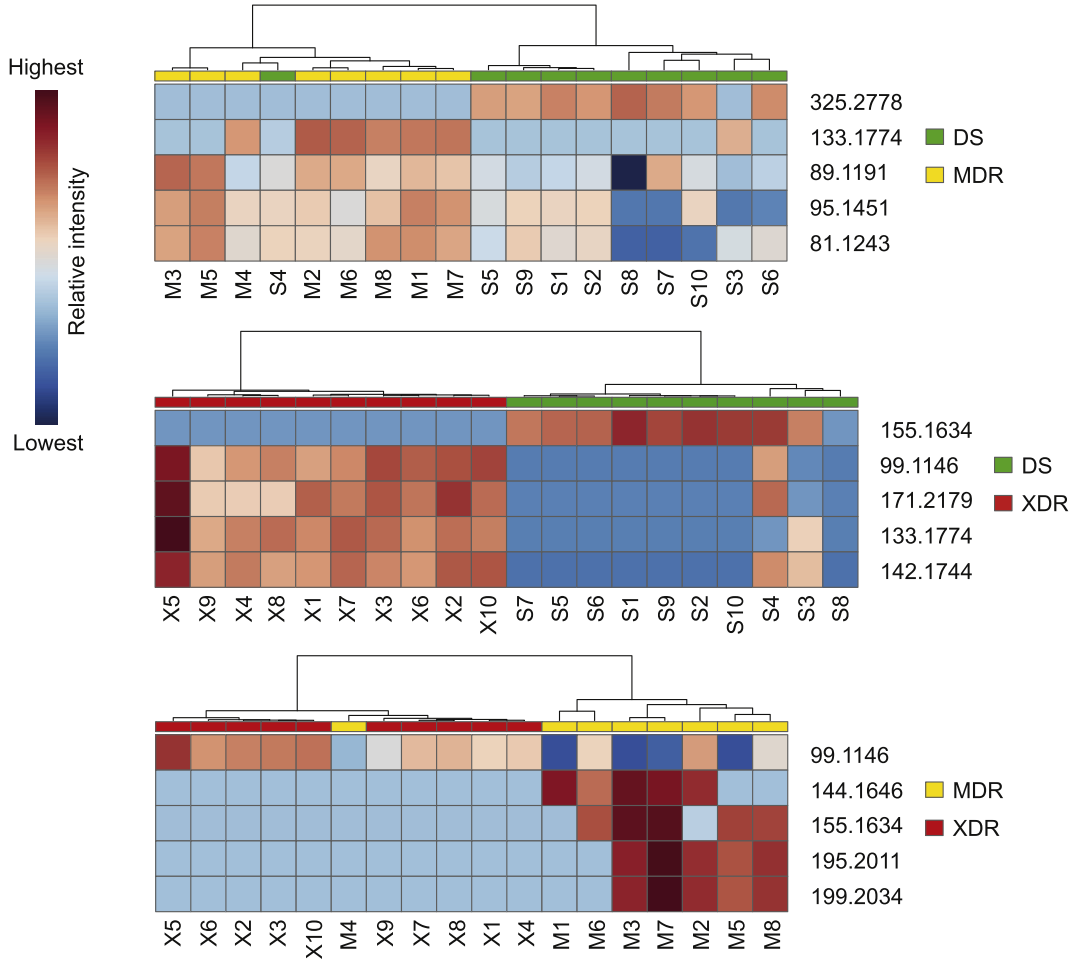

Fig. 1. Hierarchical clustering of metabolic profiles of DS, MDR, and XDR *M. tuberculosis* strains tested in Experiment A. Dendrograms and heat maps were generated using MetaboAnalyst and the 5 ions with the highest discriminatory power detected in positive ionization mode. Each line in the heatmap represents a metabolite and each column represents a strain. Metabolite intensity in each sample is represented in a standard scale from blue (lower intensity) to red (higher intensity). S, drug-susceptible strains; M, multidrugresistant strains; X, extensively drug-resistant strains. (For interpretation of the references to colour in this figure legend, the reader is referred to the Web version of this article.)

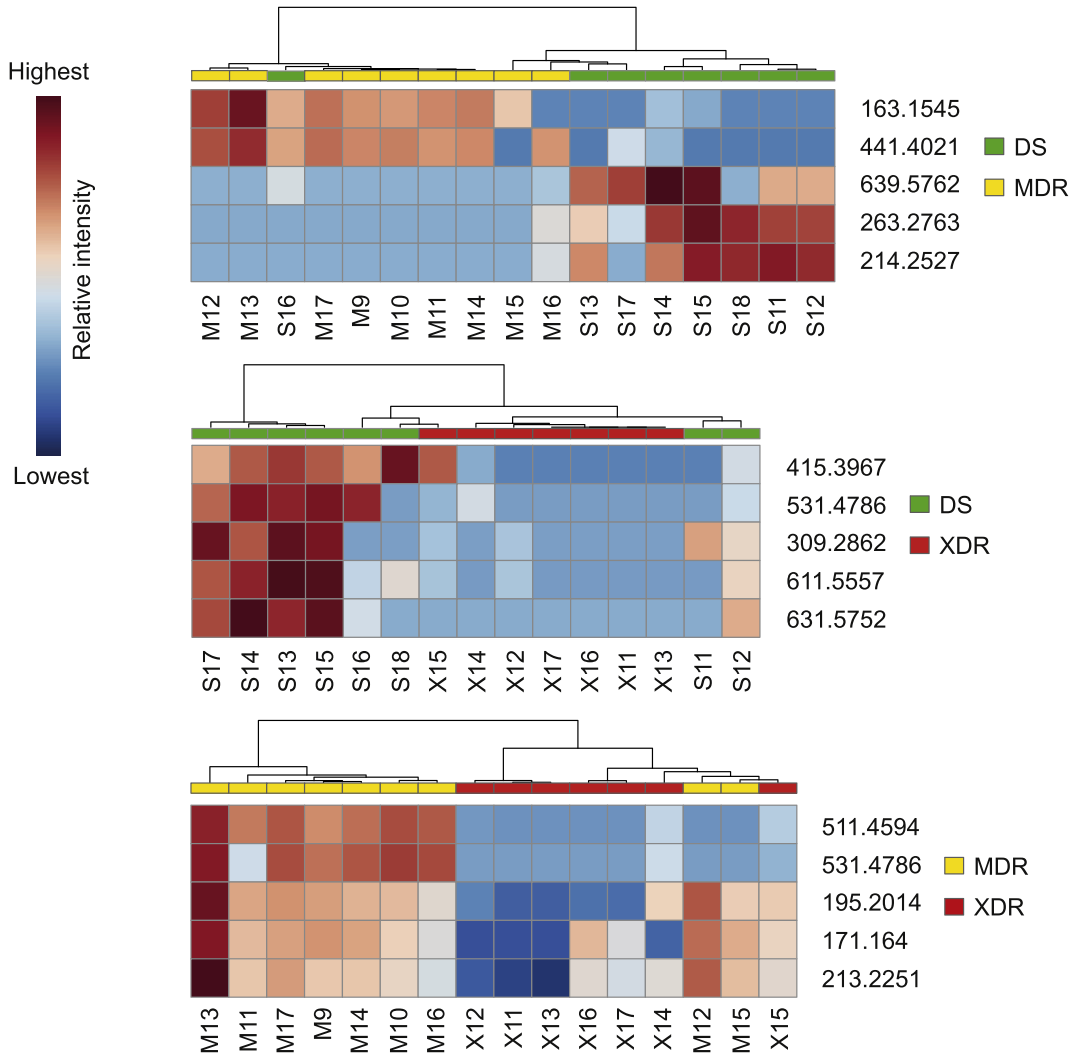

Fig. 2. Hierarchical clustering of metabolic profiles of DS, MDR, and XDR *M. tuberculosis* strains tested in Experiment B. Dendrograms and heat maps were generated using MetaboAnalyst and the 5 ions with the highest discriminatory power detected in positive ionization mode. Each line in the heatmap represents a metabolite and each column represents a strain. Metabolite intensity in each sample is represented in a standard scale from blue (lower intensity) to red (higher intensity). S, drug-susceptible strains; M, multidrugresistant strains; X, extensively drug-resistant strains. (For interpretation of the references to colour in this figure legend, the reader is referred to the Web version of this article.)

the metabolic fingerprint of sera from patients with leprosy, a disease caused by *Mycobacterium leprae* [18]. In line with this, various metabolomics studies have searched for biomarkers in the context of TB [25]. Recently, one study searched for metabolomic signatures to predict TB progression from household contacts of TB index cases as well as disease severity in a non-human primate model [26]. Also, Cho et al. (2020) studied the serum metabolome of healthy individuals, subjects with latent *M. tuberculosis* infection, and active TB cases to search for biomarkers [27]. Biomarker identification in TB is an active area of research and is not limited to metabolomics of serum samples. Mehaffy et al. used proteomics to detect specific *M. tuberculosis* peptides in serum from patients with active and latent TB [28,29]. Other studies have investigated the chemical composition of urine in search of biomarkers [30].

Based on these and other studies, we hypothesized that *M. tuberculosis* strains with different drug susceptibility profiles would be metabolically distinct, and untargeted metabolomics could reveal recognizable metabolic patterns correlated with drug susceptibility or resistance. Thus, we selected 53 *M. tuberculosis* strains and evaluated their susceptibility to first and second-line drugs (Table S2). Then, two independent, chronologically separated DI-MS analyses were performed to evaluate potential metabolic differences between DS, MDR, and XDR strains. Initially, 10 DS strains (S1–S10), 8 MDR strains (M1-M8), and 10 XDR strains (X1-X10) were selected for metabolic characterization. As described below, and due to the promising results obtained with the first strain set, a second set was later selected: 8 DS strains (S11–S18), 9 MDR strains (M9-M17), and 8 XDR strains (X11-X18) (Table S2). For clarity, these independent analyses are hereafter referred to as "Experiment A" and "Experiment B".

The strains comprising each of the strain sets were selected based on (i) availability in our collection, (ii) ability to grow from frozen stocks, and (iii) similarity regarding drug susceptibility profiles. Regarding the latter, MDR strains that were resistant to rifampicin and isoniazid but susceptible to all other drugs tested were selected, and XDR strains selected were those which were resistant to as many antibiotics as possible. Assignment to Experiment A or B was completely random, as these analyses were chronologically independent. The reason for adopting this experimental setup was to be sure that results could be obtained (i) in different mass spectrometry runs and (ii) using different sets of strains. Direct infusion mass spectrometry is highly sensitive to ion suppression, and two separate runs of the same samples will invariably produce differences in the ions detected. Therefore, although

results from a single run with all strains may present greater potential for the detection of biomarkers with more statistically robust differences, this would not be a good representation of a real-life application of the method for the diagnosis of drug resistance based on metabolic profiles.

Following DI-MS, we filtered our dataset to include only ions that were detected in at least 80% of samples of at least one group. We then analyzed these data using MetaboAnalyst and performed hierarchical clustering using all metabolites or only the 5 metabolites with the highest discriminatory power. In Experiment A, hierarchical clustering using all metabolites produced a remarkable separation between XDR and other groups in positive mode, although no significant separation was observed between MDR and DS strains (data not shown). In negative mode, we did not observe good separation between groups using all filtered metabolites (data not shown). When we considered only the 5 metabolites with the highest discriminatory power, a clear separation between all sample groups was observed in positive ionization (Fig. S1). When using the top 5 metabolites from negative mode, an excellent separation between DS and DR strains was observed, although no significant separation was observed between MDR and XDR strains (Fig. S1). Given the promising results obtained in positive ionization mode, we then characterized the second set of strains in an identical manner. In Experiment B, when the top 5 ions were considered, we observed a significant separation of MDR strains compared to DS and XDR strains. However, strains from the two other groups were completely mixed and could not be distinguished based on the top 5 ions (Fig. S2).

Results described above showed that metabolites can serve, though to a limited extent, as indicators of drug susceptibility. To determine if this strategy could achieve higher predictive power during comparisons of only two strain groups, we performed hierarchical clustering comparing two groups at a time, using positive ionization data. These analyses were carried out based on the degree of similarity of abundance profiles of the top 5 metabolites. First, we compared DS and MDR strains and found that this analysis produced an excellent separation between these groups in Experiments A and B (Figs. 1 and 2, top panels). We then compared DS and XDR strains, obtaining perfect separation in Experiment A and moderate separation in Experiment B (Figs. 1 and 2, middle panels). The final analysis compared MDR and XDR strains; again, an excellent separation between groups could be observed (Figs. 1 and 2, bottom panels). Therefore, our data on metabolic profiles of DS, MDR, and XDR strains and hierarchical clustering showed that at least some strains could be identified based on their clustering, especially in binary comparisons. It is worth noting that as few as 5 ions were required to obtain separation, suggesting that broad metabolic profiling assays may not be required to predict drug resistance.

Given that clustering of metabolomics data suggested that, although useful, phenotypical drug resistance profiles are not always associated with metabolic fingerprints, we sought to determine if differences in the occurrence of genetic determinants of resistance were responsible for some of the discrepancies observed. Therefore, we sequenced genes involved in resistance to first- and second-line drugs (*rpoB*, *katG*, *inhA*, *gyrA*, and *rrs*), searched for mutations known to be associated with drug resistance and compared results to phenotypic data. By doing so, we found apparent discrepancies between genetic and phenotypic data, where mutations associated with resistance were found in DS strains, whereas no mutations were found in some DR strains (Table S3).

Among the discordant results, we observed the absence of *rrs* mutations in strains that were phenotypically resistant to amikacin and kanamycin (X6, X9, X10, X12, X15, and X16), absence of *gyrA* mutations in one strain phenotypically resistant to ofloxacin (X15), absence of *katG* and *inhA* mutations in isoniazid-resistant strains (M6, M12, X1, X2, X14, and X7), absence of *rpoB* mutations associated with resistance in a rifampicin-resistant strain (M12) and presence of a *inhA* mutation in a phenotypically DS strain (S1). Despite these disagreements, most strains whose metabolic fingerprints did not cluster as expected did not present genotype-phenotype discrepancies. An exception to this is M4; despite

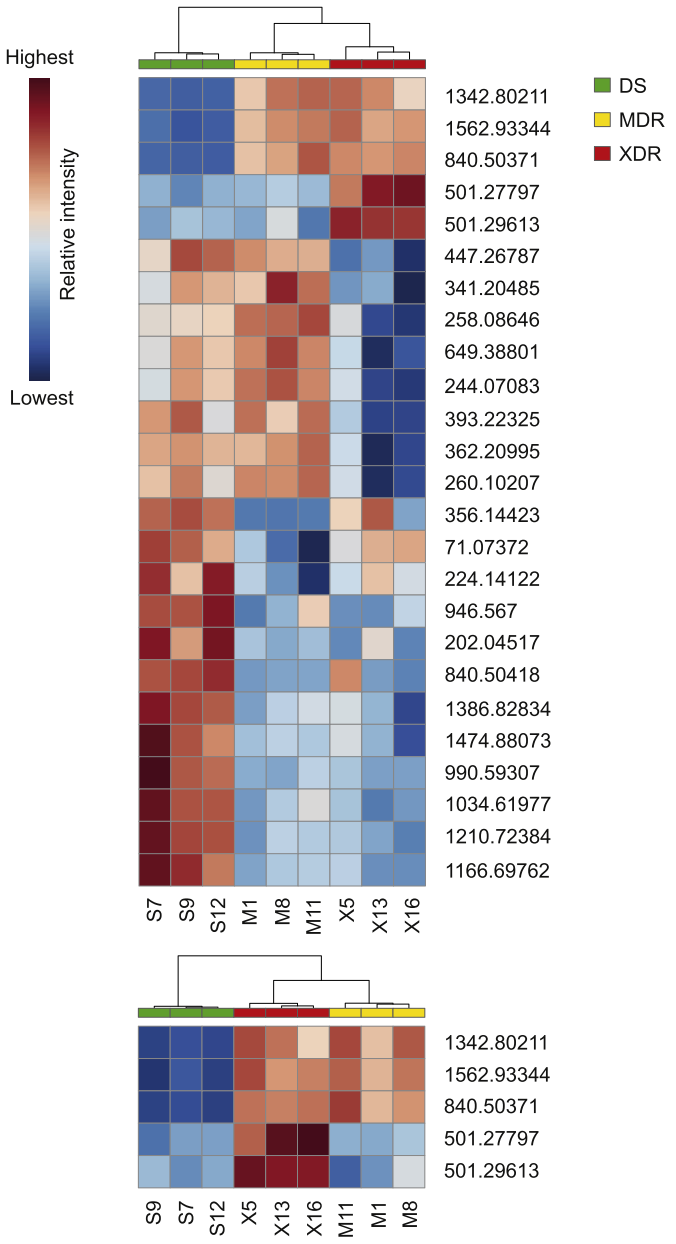

Fig. 3. Hierarchical clustering of metabolic profiles of DS, MDR, and XDR *M. tuberculosis* strains obtained by UHPLC-MS. Dendrograms and heat maps were generated using MetaboAnalyst and the 25 (top panel) or 5 (bottom panel) ions with the highest discriminatory power detected in positive ionization mode. Each line in the heatmap represents a metabolite and each column represents a strain. Metabolite intensity in each sample is represented in a standard scale from blue (lower intensity) to red (higher intensity). S, susceptible strains; M, multidrug-resistant strains; X, extensively drug-resistant strains. (For interpretation of the references to colour in this figure legend, the reader is referred to the Web version of this article.)

being (phenotypically) MDR, and sensitive to second-line drugs, it presented a mutation in *gyrA* that confers resistance to ofloxacin. Fig. S1 shows M4 grouped with XDR strains when positive ionization data was analyzed. Although this strain was phenotypically susceptible to ofloxacin, clustering with XDR strains is compatible with the presence of a resistance marker to a second-line drug.

To validate DI-MS results, we performed UHPLC-HRMS using 3 strains from each group (Table S2). For this, we chose strains that were genetically similar and whose DNA sequences corroborated phenotypic data. Metabolic data were processed as described above, and

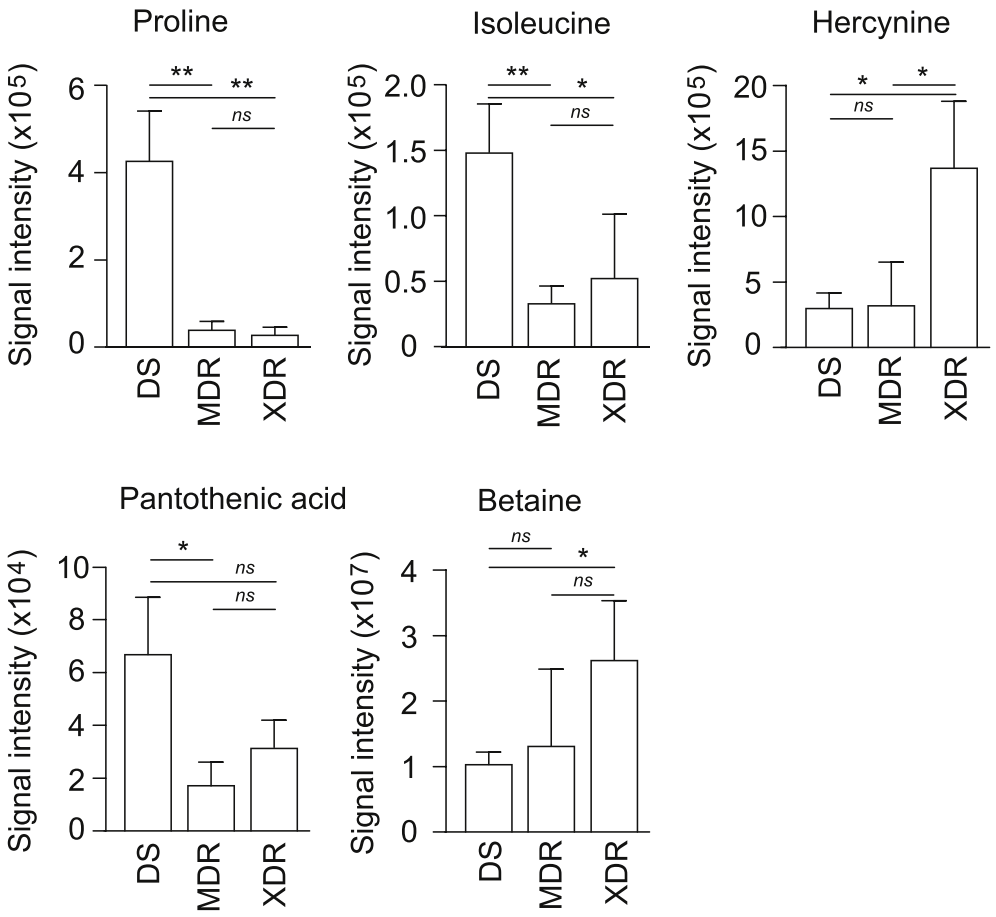

Fig. 4. Relative levels of 5 metabolites whose levels differed significantly between DS, MDR, and XDR strains. Metabolite identifications were performed by UHPLC-HRMS in positive ionization mode and comparison of collision-induced fragmentation patterns using Compound Discoverer. Compounds were selected based on ratios (and *p* values) between average signal intensities of each sample group (DS, MDR, XDR). Results shown are the averages of measurements from three strains, and bars indicate the standard deviations. DS, drug-susceptible strains; MDR, multidrug-resistant strains; XDR, extensively drug-resistant strains. *ns*: not statistically significant. *$p < 0.05$; **$p < 0.01$; ***$p < 0.001$; ****$p < 0.0001$.

dendrograms were generated using the 25 and 5 metabolites with the highest discriminatory power. By doing so, we observed a remarkable separation between the three groups (Fig. 3). As previously, we also performed binary analyses based on the top 5 metabolites. As expected, clustering was entirely congruent with phenotypic DST profiles (data not shown).

In addition to parental *m/z* detection, we performed collision-induced dissociation and analyzed daughter ions, allowing us to obtain putative identities through comparisons of fragmentation profiles. We then selected a few compounds based on 3 criteria: highest signal intensity ratios, statistically significant ($p < 0.05$) differences in levels between strain groups and putative identities with simple chemical nature. By doing so, we attempted to select compounds that hold significant discriminatory power and molecular characteristics that would allow detection by simple methods. As a result, levels of isoleucine, proline, hercynine, betaine, and pantothenic acid were compared between groups, showing that relative levels of these metabolites varied significantly (Fig. 4).

As shown in Fig. 4, levels of a metabolite presumptively identified as pantothenic acid were significantly higher in DS strains. Pantothenic acid is essential for the synthesis of coenzyme A and acyl carrier protein, which play important roles as carriers of acyl groups in fatty acid metabolism, in the tricarboxylic acid cycle (TCA), and other reactions of intermediate metabolism [31]. Virtually nothing can be found in the literature regarding the role of pantothenic acid in drug resistance in *M. tuberculosis*. However, using metabolomics, Lau et al. (2015) have described the presence of high levels of dexpanthenol, the alcohol analog of pantothenic acid, in cultures of *M. tuberculosis* strains, as compared to non-tuberculous mycobacteria [32].

Besides pantothenic acid, higher levels of hercynine and betaine were detected in XDR strains. Hercynine catalysis is an intermediate step in the biosynthesis of ergothioneine, which in turn is one of the major redox buffers that protect bacteria against oxidative agents, in addition to regulating microbial physiology, cell metabolism and pathogenesis [33,34]. Therefore, it is possible that the accumulation of hercynine is due to the high demand for ergothioneine synthesis to combat the high oxidative stress that may result from drug resistance mutations, which lie in genes critical for bacterial survival, having effects on important cellular processes. One such gene is *rpoB*, and it is worth noting that rifampicin inhibits transcription of bacterial DNA by binding to the RNA polymerase subunit encoded by this gene [35,36]. Although very little can be found in the literature about the role of hercynine in *M. tuberculosis*, Saini and colleagues (2016) have studied the role of the related compound ergothioneine in drug susceptibility and oxidative stress in this organism. Their data confirm the central role of ergothioneine in the control of endogenous reactive oxygen species and in the protection of *M. tuberculosis* against diverse oxidative stressors, such as hydrogen peroxide, paraquat, menadione, and cumene hydroperoxide. Of particular relevance to our data, Saini and colleagues demonstrated that a mutant with compromised ability to synthesize ergothioneine shows increased susceptibility to rifampicin, isoniazid, bedaquiline, and clofazimine, confirming the involvement of this compound in pathways that affect phenotypic drug resistance [37].

Data presented herein corroborate studies of *rpoB* mutations and their relationship with fatty acid metabolism. Du Preez and Loots demonstrated that *rpoB* mutants showed reduced synthesis of certain branched chain fatty acids required for mycolic acid synthesis [11]. In another study, authors observed a total loss of aconitic acid in *rpoB* mutants, disrupting the functionality of the enzyme aconitase, important in the TCA and in the stabilization and protection of mRNA against degradation during conditions of low iron concentration or oxidative stress [38]. Another important finding in *rpoB* mutants was the

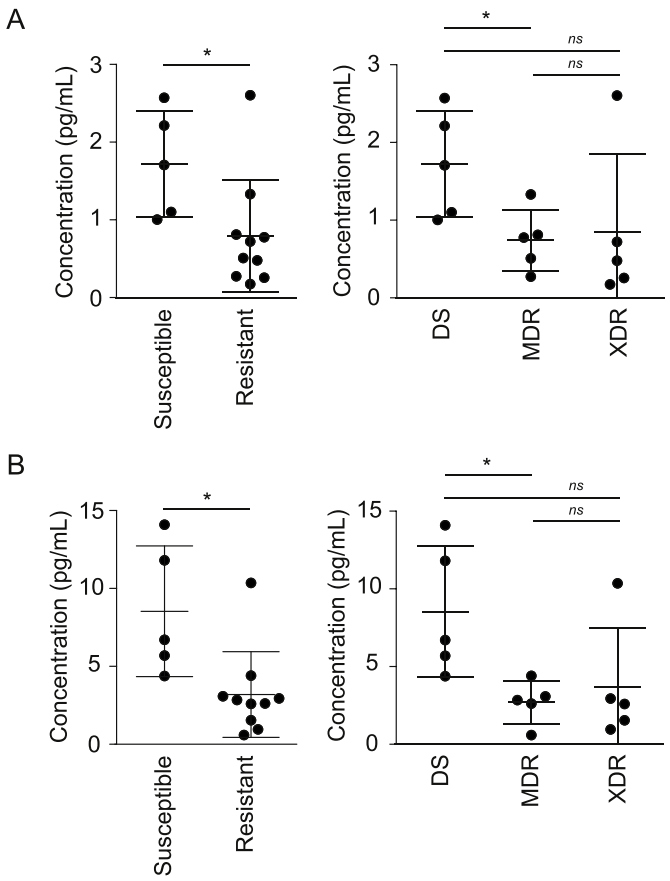

Fig. 5. Absolute levels of proline and isoleucine in metabolite extracts from DS, MDR, and XDR strains. Pure standard compounds were analyzed by UHPLC-MS in positive ionization mode and standard curves were produced using known concentrations and MS signal intensity values. MS signal intensities of appropriate ions in sample extracts were fitted to curves to obtain absolute concentrations. Proline (A) and isoleucine (B) concentrations are shown. Each dot represents one *M. tuberculosis* strain, whereas lines represent averages and standard deviations. DS, drug-susceptible strains; MDR, multidrug-resistant strains; XDR, extensively drug-resistant strains. *ns*: not statistically significant. *$p < 0.05$.

reduction of cell wall synthesis capacity, directly interfering with cellular homeostasis and oxidative stress. Confirming these findings, Loots found alterations in several metabolites related to cell wall maintenance in a rifampicin-resistant mutant [38]. These findings were in line with those reported by Bisson et al., and this reduction can be explained by positive regulation of phthiocerol dymicocerosates synthesis in an attempt to maintain or remodel the cell wall [39]. In 2014, Loots identified novel metabolic pathways and biomarkers comparing metabolite profiles of wild-type and isoniazid-resistant strains. High concentrations of metabolites associated with oxidative stress were found, and a higher susceptibility to oxidative stress in isoniazid-resistant strains was observed [12]. Therefore, lower levels of pantothenic acid in resistant strains and the consequent reduction in coenzyme A and acyl carrier protein synthesis may directly interfere in the synthesis of mycolic acid, an important cell wall component.

Although to our knowledge no other studies comparing the metabolome of DS, MDR, and XDR *M. tuberculosis* clinical strains have been published, Huang and colleagues used metabolomics to compare serum samples from healthy controls, DS-TB and MDR-TB patients [40]. Metabolites that distinguished MDR-TB from DS-TB and healthy control samples included N1-methyl-2-pyridone-5-carboxamide, 1-myristoyl-sn-glycerol-3-phosphocholine, caprylic acid, and D-xylulose. Additionally, pathway enrichment analysis suggested phospholipid cell membrane remodeling is an important feature of MDR-TB, results that are somewhat reminiscent of the ones described herein.

Having identified multiple metabolites whose levels serve as indicators of drug susceptibility, we determined absolute concentrations of proline and isoleucine in DS, MDR and XDR strains through UHPLC-MS. Although relative levels of these compounds did not allow differentiation between MDR and XDR strains (Fig. 4), these metabolites were chosen due to their stability and potential for detection using simple biochemical methods, making them interesting targets for the development of biomarkers. Therefore, we produced standard curves for proline and isoleucine and compared signal intensities from ions detected in *M. tuberculosis* extracts to determine absolute concentrations. Results confirmed that both proline and isoleucine levels vary depending on drug susceptibility profiles (Fig. 5). As expected, MDR and XDR strains did not differ significantly regarding levels of these metabolites. However, levels of both amino acids were significantly different when DS and MDR strains were compared. In general, DS and XDR strains also showed profiles that looked clearly different, although this difference was not statistically significant owing to the presence of one outlier in the XDR group. Nevertheless, when we divided our strains in DS and DR groups, a statistically-significant difference in metabolite levels was observed. Both isoleucine and proline showed significantly higher levels in DS strains when compared to their DR counterparts (Fig. 5).

Future work will focus on the analysis of larger groups of strains. It is important to point out that categorization of samples in MDR or XDR groups relies on DST of qualitative nature. The BACTEC MGIT System relies on O_2 consumption by growing cultures. Once a culture reaches a growth threshold in the presence of an antibiotic it is considered "resistant". However, strains that grow significantly well in the presence of an antibiotic without reaching that threshold are common. Determination of minimum inhibitory concentrations for antibiotics and strains used herein may shed light on some apparent discrepancies found in our results. Limitations notwithstanding, our data show that metabolic markers of drug resistance can be found through metabolomics, and that simple metabolites may be used to differentiate strains regarding drug susceptibility profiles. Additionally, our data add to the current understanding of the effect of drug resistance on bacterial metabolism, and highlights the importance of fatty acid and mycolic acid metabolism, essential for cell wall structure and the response to oxidative stress in *M. tuberculosis*.

Author contribution

Amanda Mendes Rêgo and L. Caetano M. Antunes: ***Conceptualization***.

Fabio Cesar S. Nogueira, Rosana B. R. Ferreira and L. Caetano M. Antunes: ***Data curation***.

Amanda Mendes Rêgo, Duanne Alves da Silva, Nicole Victor Ferreira, Lucindo Cardoso de Pina, Joseph A. M. Evaristo, Geisa P. Caprini Evaristo, Soraya M. Ochs, Julio J. Amaral: ***Formal analysis***.

Rosana B. R. Ferreira and L. Caetano M. Antunes: ***Funding acquisition***.

Amanda Mendes Rêgo, Duanne Alves da Silva, Nicole Victor Ferreira, Lucindo Cardoso de Pina, Joseph A. M. Evaristo, Geisa P. Caprini Evaristo, Soraya M. Ochs, Julio J. Amaral, Fabio Cesar S. Nogueira, Rosana B. R. Ferreira and L. Caetano M. Antunes: ***Investigation***.

Amanda Mendes Rêgo, Joseph A. M. Evaristo, Geisa P. Caprini Evaristo, Fabio Cesar S. Nogueira, Soraya M. Ochs, Julio J. Amaral, Rosana B. R. Ferreira and L. Caetano M. Antunes: ***Methodology***.

Rosana B. R. Ferreira and L. Caetano M. Antunes: ***Project administration***.

Fabio Cesar S. Nogueira, Julio J. Amaral, Rosana B. R. Ferreira and L. Caetano M. Antunes: ***Resources***.

Fabio Cesar S. Nogueira and Julio J. Amaral: ***Software***.

Fabio Cesar S. Nogueira, Rosana B. R. Ferreira and L. Caetano M.

Antunes: ***Supervision***.

Amanda Mendes Rêgo and L. Caetano M. Antunes: ***Writing - original draft***.

Amanda Mendes Rêgo, Duanne Alves da Silva, Nicole Victor Ferreira, Lucindo Cardoso de Pina, Joseph A. M. Evaristo, Geisa P. Caprini Evaristo, Fabio Cesar S. Nogueira, Soraya M. Ochs, Julio J. Amaral, Rosana B. R. Ferreira and L. Caetano M. Antunes: ***Writing - review & editing***.

Funding

This study was supported by Fundação Carlos Chagas Filho de Amparo à Pesquisa do Estado do Rio de Janeiro (FAPERJ), Conselho Nacional de Desenvolvimento Científico e Tecnológico (CNPq), Coordenação de Aperfeiçoamento de Pessoal de Nível Superior (CAPES) (Finance Code 001), as well as Fundação Oswaldo Cruz.

Declaration of competing interest

None to declare.

Appendix A. Supplementary data

Supplementary data to this article can be found online at https://doi.org/10.1016/j.tube.2020.102043.

References

[1] WHO. World health organization. Global tuberculosis report. 2017.
[2] WHO. World health organization. Global tuberculosis report. 2019.
[3] Zhang Y, Yew WW. Mechanisms of drug resistance in Mycobacterium tuberculosis. Int J Tubercul Lung Dis 2009;13:1320–30.
[4] Canetti G, Froman S, Grosset J, Hauduroy P, Langerova M, Mahler HT, Meissner G, Mitchison DA, Sula L. Mycobacteria: Laboratory methods for testing drug sensitivity and resistance. Bull World Health Organ 1963;29:565–78.
[5] Siddiqi SH, Rüsch-Gerdes. S. MGITTM procedure manual for BACTEC™ MGIT 960™ TB System. FIND. 2006.
[6] Swanepoel CC, Loots dT. The use of functional genomics in conjunction with metabolomics for *Mycobacterium tuberculosis* research. Dis Markers 2014;2014:124218.
[7] Farhat MR, Shapiro BJ, Kieser KJ, Sultana R, Jacobson KR, Victor TC, Warren RM, Streicher EM, Calver A, Sloutsky A, Kaur D, Posey JE, Plikaytis B, Oggioni MR, Gardy JL, Johnston JC, Rodrigues M, Tang PK, Kato-Maeda M, Borowsky ML, Muddukrishna B, Kreiswirth BN, Kurepina N, Galagan J, Gagneux S, Birren B, Rubin EJ, Lander ES, Sabeti PC, Murray M. Genomic analysis identifies targets of convergent positive selection in drug-resistant Mycobacterium tuberculosis. Nat Genet 2013;45:1183–9.
[8] Borrell S, Gagneux S. Infectiousness, reproductive fitness and evolution of drug-resistant Mycobacterium tuberculosis. Int J Tubercul Lung Dis 2009;13:1456–66.
[9] Kempf I, Zeitouni S. [The cost of antibiotic resistance: analysis and consequences]. Pathol Biol 2012;60:e9–14.
[10] Kodio O, Georges Togo AC, Sadio Sarro YD, Fane B, Diallo F, Somboro A, Degoga B, Kone M, Coulibaly G, Tolofoudje M, Bane S, Sanogo M, Kone B, Coulibaly N, Dabitao D, Baya B, Maiga M, Bougoudogo F, Samake F, Dao S, Doumbia S, Diallo S, Diarra B. Competitive fitness of. Int J Mycobacteriol 2019;8:287–91.
[11] du Preez I, Loots dT. Altered fatty acid metabolism due to rifampicin-resistance conferring mutations in the *rpoB* gene of *Mycobacterium tuberculosis*: mapping the potential of pharmaco-metabolomics for global health and personalized medicine. OMICS 2012;16:596–603.
[12] Loots dT. An altered *Mycobacterium tuberculosis* metabolome induced by *katG* mutations resulting in isoniazid resistance. Antimicrob Agents Chemother 2014;58:2144–9.
[13] Nandakumar M, Nathan C, Rhee KY. Isocitrate lyase mediates broad antibiotic tolerance in *Mycobacterium tuberculosis*. Nat Commun 2014;5:4306.
[14] Jansen RS, Rhee KY. Emerging approaches to tuberculosis drug development: at home in the metabolome. Trends Pharmacol Sci 2017;38:393–405.
[15] Pires ES, Hardoim CCP, Miranda KR, Secco DA, Lobo LA, de Carvalho DP, Han J, Borchers CH, Ferreira RBR, Salles JF, Domingues RMCP, Antunes LCM. The gut microbiome and metabolome of two riparian communities in the amazon. Front Microbiol 2019;10:2003.
[16] Mattos KA, Oliveira VC, Berrêdo-Pinho M, Amaral JJ, Antunes LC, Melo RC, Acosta CC, Moura DF, Olmo R, Han J, Rosa PS, Almeida PE, Finlay BB, Borchers CH, Sarno EN, Bozza PT, Atella GC, Pessolani MC. Mycobacterium leprae intracellular survival relies on cholesterol accumulation in infected macrophages: a potential target for new drugs for leprosy treatment. Cell Microbiol 2014;16:797–815.
[17] Antunes LC, Han J, Pan J, Moreira CJ, Azambuja P, Borchers CH, Carels N. Metabolic signatures of triatomine vectors of Trypanosoma cruzi unveiled by metabolomics. PloS One 2013;8:e77283.
[18] Amaral JJ, Antunes LC, de Macedo CS, Mattos KA, Han J, Pan J, Candéa AL, Henriques M, Ribeiro-Alves M, Borchers CH, Sarno EN, Bozza PT, Finlay BB, Pessolani MC. Metabonomics reveals drastic changes in anti-inflammatory/pro-resolving polyunsaturated fatty acids-derived lipid mediators in leprosy disease. PLoS Neglected Trop Dis 2013;7:e2381.
[19] Arena ET, Auweter SD, Antunes LC, Vogl AW, Han J, Guttman JA, Croxen MA, Menendez A, Covey SD, Borchers CH, Finlay BB. The deubiquitinase activity of the Salmonella pathogenicity island 2 effector, SseL, prevents accumulation of cellular lipid droplets. Infect Immun 2011;79:4392–400.
[20] Antunes LC, Andersen SK, Menendez A, Arena ET, Han J, Ferreira RB, Borchers CH, Finlay BB. Metabolomics reveals phospholipids as important nutrient sources during Salmonella growth in bile in vitro and in vivo. J Bacteriol 2011;193:4719–25.
[21] Antunes LC, Finlay BB. A comparative analysis of the effect of antibiotic treatment and enteric infection on intestinal homeostasis. Gut Microb 2011;2:105–8.
[22] Antunes LC, Arena ET, Menendez A, Han J, Ferreira RB, Buckner MM, Lolic P, Madilao LL, Bohlmann J, Borchers CH, Finlay BB. Impact of *Salmonella* infection on host hormone metabolism revealed by metabolomics. Infect Immun 2011;79:1759–69.
[23] Antunes LC, Han J, Ferreira RB, Lolić P, Borchers CH, Finlay BB. Effect of antibiotic treatment on the intestinal metabolome. Antimicrob Agents Chemother 2011;55:1494–503.
[24] Han J, Antunes LC, Finlay BB, Borchers CH. Metabolomics: towards understanding host-microbe interactions. Future Microbiol 2010;5:153–61.
[25] du Preez I, Luies L, Loots DT. The application of metabolomics toward pulmonary tuberculosis research. Tuberculosis 2019;115:126–39.
[26] Duffy FJ, Weiner J, Hansen S, Tabb DL, Suliman S, Thompson E, Maertzdorf J, Shankar S, Tromp G, Parida S, Dover D, Axthelm MK, Sutherland JS, Dockrell HM, Ottenhoff THM, Scriba TJ, Picker LJ, Walzl G, Kaufmann SHE, Zak DE, Consortium G. Immunometabolic signatures predict risk of progression to active tuberculosis and disease outcome. Front Immunol 2019;10:527.
[27] Cho Y, Park Y, Sim B, Kim J, Lee H, Cho SN, Kang YA, Lee SG. Identification of serum biomarkers for active pulmonary tuberculosis using a targeted metabolomics approach. Sci Rep 2020;10:3825.
[28] Mehaffy C, Kruh-Garcia NA, Graham B, Jarlsberg LG, Willyerd CE, Borisov A, et al. Identification of. J Clin Microbiol 2020;58:e00393–20. https://doi.org/10.1128/JCM.00393-20.
[29] Kruh-Garcia NA, Wolfe LM, Chaisson LH, Worodria WO, Nahid P, Schorey JS, Davis JL, Dobos KM. Detection of Mycobacterium tuberculosis peptides in the exosomes of patients with active and latent M. tuberculosis infection using MRM-MS. PloS One 2014;9:e103811.
[30] Combrink M, du Preez I, Ronacher K, Walzl G, Loots DT. Time-dependent changes in urinary metabolome before and after intensive phase tuberculosis therapy: a pharmacometabolomics study. OMICS 2019;23:560–72.
[31] Sambandamurthy VK, Wang X, Chen B, Russell RG, Derrick S, Collins FM, Morris SL, Jacobs WR. A pantothenate auxotroph of Mycobacterium tuberculosis is highly attenuated and protects mice against tuberculosis. Nat Med 2002;8:1171–4.
[32] Lau SK, Lam CW, Curreem SO, Lee KC, Lau CC, Chow WN, Ngan AH, To KK, Chan JF, Hung IF, Yam WC, Yuen KY, Woo PC. Identification of specific metabolites in culture supernatant of *Mycobacterium tuberculosis* using metabolomics: exploration of potential biomarkers. Emerg Microb Infect 2015;4:e6.
[33] Ta P, Buchmeier N, Newton GL, Rawat M, Fahey RC. Organic hydroperoxide resistance protein and ergothioneine compensate for loss of mycothiol in Mycobacterium smegmatis mutants. J Bacteriol 2011;193:1981–90.
[34] Cumming BM, Chinta KC, Reddy VP, Steyn AJC. Role of ergothioneine in microbial physiology and pathogenesis. Antioxidants Redox Signal 2018;28:431–44.
[35] Olivier I, Loots D. An overview of tuberculosis treatment and diagnostics. What role could metabolomics play? J Cell Tissue Res 2011;11.
[36] Telenti A, Imboden P, Marchesi F, Lowrie D, Cole S, Colston MJ, Matter L, Schopfer K, Bodmer T. Detection of rifampicin-resistance mutations in *Mycobacterium tuberculosis*. Lancet 1993;341:647–50.
[37] Saini V, Cumming BM, Guidry L, Lamprecht DA, Adamson JH, Reddy VP, Chinta KC, Mazorodze JH, Glasgow JN, Richard-Greenblatt M, Gomez-Velasco A, Bach H, Av-Gay Y, Eoh H, Rhee K, Steyn AJC. Ergothioneine maintains redox and bioenergetic homeostasis essential for drug susceptibility and virulence of *Mycobacterium tuberculosis*. Cell Rep 2016;14:572–85.
[38] Loots dT. New insights into the survival mechanisms of rifampicin-resistant *Mycobacterium tuberculosis*. J Antimicrob Chemother 2016;71:655–60.
[39] Bisson GP, Mehaffy C, Broeckling C, Prenni J, Rifat D, Lun DS, Burgos M, Weissman D, Karakousis PC, Dobos K. Upregulation of the phthiocerol dimycocerosate biosynthetic pathway by rifampin-resistant, *rpoB* mutant *Mycobacterium tuberculosis*. J Bacteriol 2012;194:6441–52.
[40] Huang H, Han YS, Chen J, Shi LY, Wei LL, Jiang TT, Yi WJ, Yu Y, Li ZB, Li JC. Highlight article: the novel potential biomarkers for multidrug-resistance tuberculosis using UPLC-Q-TOF-MS. Exp Biol Med 2020;245:501–11.